Latin American Journal of Solids and Structures
www.lajss.org

Finite element modelling to assess the effect of position and size of the piezoelectric layer of a hybrid beam

Abstract
A one dimensional finite element model is presented to assess the effect of position and size of the piezoelectric layer of a hybrid beam. The efficient layerwise (zigzag) theory is used for making the finite element model. The 1D beam element has eight mechanical and a variable number of electrical degrees of freedom. The codes are developed in Matlab based on the FE formulation. The beams are also modelled in 2D planar modelling space as a deformable shell using FE package ABAQUS for comparison of results. An 8-noded piezoelectric quadrilateral element is used for piezo layers and an 8-noded quadrilateral element with reduced integration is used for the elastic layers of hybrid beams for making the finite element mesh in ABAQUS. The accuracy of the used elements are assessed for static response. Cantilever hybrid beams with a piezoelectric layer bonded on top of the elastic substrate are considered for the analysis. The beams are subjected to electromechanical loading. A detailed study is conducted to highlight the influence of positon and size of piezoelectric layer on the deflection profiles, tip deflections and through the thickness distribution of displacements and stresses of hybrid composite/sandwich beams. The shape control using various numbers of piezoelectric patches is also studied. The 1D-FE results are compared with the 2D-FE results.

Keywords
Zigzag Theory, FEM, Hybrid Beam, ABAQUS, Piezoelectric patch, shape control.

Najeeb ur Rahman [a]*
M. Naushad Alam [a]

[a]Department of Mechanical Engineering, Zakir Husain College of Engineering and Technology - Z.H.C.E.T, Aligarh Muslim University - A. M. U, Aligarh, Uttar Pradesh, India. E-mail: najeebalig@rediffmail.com, naushad7863@rediffmail.com

*Corresponding author

http://dx.doi.org/10.1590/1679-78253959

Received: April 25, 2017
In Revised Form: October 06, 2017
Accepted: October 17, 2017
Available online: February 05, 2018

1 INTRODUCTION

Smart multi-layered hybrid beams with some sensory and actuator piezoelectric layers constitute an important element of adaptive structures. These structural systems are generally made of composite and sandwich laminates because of their high stiffness to weight ratio. Considerable attention has been received in literature on behaviour of hybrid smart structures and reviewed by many researchers (Benjeddou, 2000; Sunar and Rao, 1999; Saravanos and Heyliger, 1999; Tang et al., 1996). Saravanos and Heyliger (1995) developed a Unified mechanics with the capability to model both sensory and active composite laminates with embedded piezoelectric layers. Layerwise formulations enable analysis of both global and local electromechanical response. They presented an approximate finite element solutions for the static and free vibration analysis of beams. But the computational effort increases with the number of layers. Many researchers used Equivalent single layer theory approximations (Correia et al., 2000; Mitchell and Reddy, 1995) for the structural analysis. Since the same global variation of displacement is assumed across the thickness independent of material properties and lay-up, such analysis fails to report the zigzag nature of in-plane displacements variations.

Few studies on structural analysis of laminates used higher-order/layer-wise theories assuming through the thickness variation for the electric field of piezoelectric layers (Batra and Vidoli, 2002; Fukunaga et al., 2001; Yang, 1999). Kapuria et al. (2004) developed a two noded finite element model for static electromechanical analysis of hybrid beam based on efficient coupled zigzag theory (Kapuria et al., 2003). Ganapathi et al. (2004) developed a C^1 finite element for the bending and torsional analysis of piezoelectric composite beams. Their formulation includes transverse shear, warping due to torsion, and elastic–electric coupling effects. Kapuria and Hagedorn (2007) presented a unified coupled efficient layerwise theory for smart beams and developed a finite element which has two physical nodes and an electric node for the electric potentials of the electroded surfaces. The

consideration of electric nodes result in significant reduction in the number of electric degrees of freedom. Rahman and Alam (2012, 2014, 2015) used layerwise (zigzag) theory for 1D-FE modelling of smart laminated beam. Kapuria and Kulkarni (2008) proposed an efficient four-node quadrilateral element using zigzag theory for the dynamic analysis of hybrid plates with segmented piezoelectric sensors and actuators. The theory considers a third-order zigzag approximation for inplane displacements, a layerwise quadratic approximation for the electric potential and a layerwise variation of the deflection to account for the piezoelectric transverse normal strain. Catapano et al. (2011) adopted Carrera's Unified Formulation for linear static analysis of composite beams. They used an N-order polynomial approximation of the displacement unknown variables to impose kinematic field above the cross-section. Komeili et al. (2011) presented the static bending analysis of functionally graded piezoelectric beams under thermo-electro-mechanical load. They derived the governing equations from Hamilton's principle and used the finite element method and Fourier series method as solution technique. Filippi et al. (2015) presented a new class of refined beam theories for static and dynamic analysis of composite structures. They implemented higher-order expansions of Chebyshev polynomials for the displacement field components over the beam cross-section. Sayyad et al. (2015b) developed a trigonometric beam theory for the bending analysis of laminated composite and sandwich beams. They considered transverse displacement as a sum of two partial displacements in their formulation. Trigonometric function is used in terms of thickness coordinate in the axial displacement field to incorporate the effect of transverse shear deformation. In another study the parabolic function is used to include this effect (Sayyad et al., 2015a). Giunta et al. (2016) used a mesh-free strong-form solution to examine the static response of functionally graded beams. They derived algebraic system via collocation with multiquadric radial basis functions.

After exhaustive literature survey it can be concluded that lots of results are available for composite beams based on various theories. But the most recent efficient zigzag theory has still some scope. In the reported literature various aspects of zigzag theory has not been studied. The shape control of structure is also very important in applications such as antennas mounted on airplane or satellites, where a small distortion in shape or surface errors result in degraded performance causing significant difficulties with respect to its usability. Modern applications require smart behaviour of structures. Piezoelectric layers often form an integral part of such smart structure owing to their ability to transform electrical energy to mechanical energy and vice versa. The location and size of these layers is significant as it results in different structural response under various loading conditions. Finite Element model to assess the effect of position and size of piezoelectric layer of a hybrid beam under static electromechanical loading is presented in this work. The efficient layerwise (zigzag) theory (Kapuria et al., 2004) is reframed for making the finite element model of hybrid beam with segmented piezoelectric patches. The codes are developed in Matlab based on the FE formulation. Static response are obtained for three different load cases for different positions and sizes of piezoelectric layer bonded on top surface of the beam. The shape control is also obtained using various numbers of piezoelectric patches. The results are presented for thin and moderately thick composite/sandwich beams. To show the accuracy of the present formulation, the 1D-FE results are compared with the 2D-FE results obtained using plane stress element in ABAQUS.

2 GOVERNING EQUATIONS FOR HYBRID PIEZOELECTRIC BEAM

Consider a hybrid beam with piezoelectric patches bonded to its surfaces. The beam is divided into segments due to the presence of these patches of variable size positioned at variable axial locations (Figure 1). The hybrid segments have piezoelectric patches bonded to the surface of elastic substrate however the elastic segments are without these patches and constitute of the elastic substrate only. As a result, the thickness of beam, number of layers across the thickness and top and bottom surfaces at any section may differ segment-wise along the length. The plane which is the mid-plane for most of the length of the beam is identified as the xy plane. At any section, z_0 is the thickness coordinate of the bottom surface and z_N is the thickness coordinate of the top surface. All the layers are considered to be perfectly bonded. The beam is transversely loaded. The load distribution is independent of the width coordinate. The $z-$axis is the poling direction for piezoelectric layers.

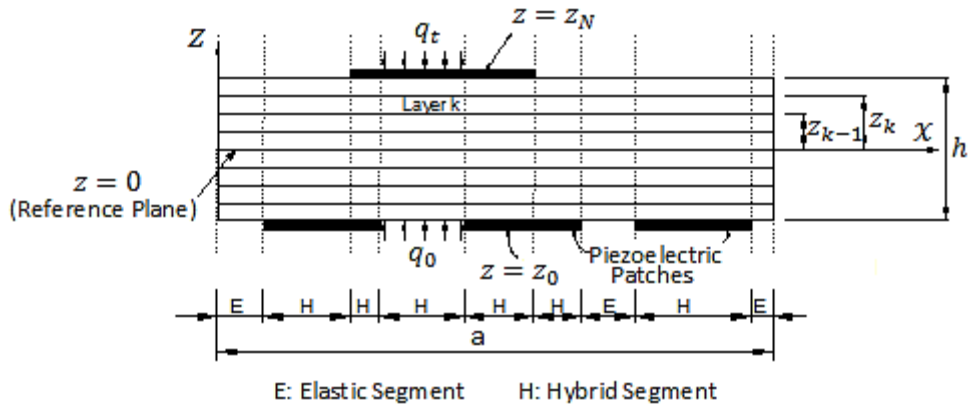

Figure 1: *Geometry of hybrid beam divided into elastic and hybrid segments*

Using coupled zigzag theory approximations (Kapuria et al., 2004) for a piezoelectric medium, the constitutive equations relating the stresses (σ_x, σ_{zx}) and electric displacements (D_x, D_z) with the strains ($\varepsilon_x, \gamma_{zx}$) and electric fields ($E_x, E_z$) are given by:

$$\begin{Bmatrix} \sigma_x \\ \sigma_{zx} \end{Bmatrix} = \begin{bmatrix} \hat{Q}_{11} & 0 \\ 0 & \hat{Q}_{55} \end{bmatrix} \begin{Bmatrix} \varepsilon_x \\ \gamma_{zx} \end{Bmatrix} - \begin{bmatrix} 0 & \hat{e}_{31} \\ \hat{e}_{15} & 0 \end{bmatrix} \begin{Bmatrix} E_x \\ E_z \end{Bmatrix}$$
$$\begin{Bmatrix} D_x \\ D_z \end{Bmatrix} = \begin{bmatrix} 0 & \hat{e}_{15} \\ \hat{e}_{31} & 0 \end{bmatrix} \begin{Bmatrix} \varepsilon_x \\ \gamma_{zx} \end{Bmatrix} + \begin{bmatrix} \hat{\eta}_{11} & 0 \\ 0 & \hat{\eta}_{33} \end{bmatrix} \begin{Bmatrix} E_x \\ E_z \end{Bmatrix} \tag{1}$$

where $\hat{Q}_{11}$ and $\hat{Q}_{55}$ are the coefficients of reduced stiffnesses; $\hat{e}_{31}$ and $\hat{e}_{15}$ are stress constants of piezoelectric material and $\hat{\eta}_{11}$ and $\hat{\eta}_{33}$ are the electric permittivities. The potential field is approximated (Kapuria et al., 2004) as

$$\phi(x,z) = \xi_\phi^l(z)\phi^l(x) \tag{2}$$

where $\phi^l(x) = \phi\left(x, z_\phi^l\right)$, $\xi_\phi^l(z)$ are linear interpolation functions for ϕ.

Considering only electric contribution in transverse strain, ε_z (Kapuria et al., 2004) and integrating it through the thickness, the deflection u_z is estimated as

$$u_z(x,z) = u_{z_0}(x) - \bar{\xi}_\phi^l(z)\phi^l(x) \tag{3}$$

where $u_{z_0}(x)$ is the deflection of mid-plane (z=0) defined as $u_{z_0}(x) = u_{z_0}(x,0)$ and $\bar{\xi}_\phi^l(z)$ is a piecewise linear function given by $\bar{\xi}_\phi^l(z) = \int_0^z d_{33} \frac{d\xi_\phi^l(z)}{dz} dz$.

The axial displacement u_x is approximated (Kapuria et al., 2004) as

$$u_x(x,z) = u_{x_0}(x) - z\frac{\partial u_{z_0}}{\partial x}(x) + S^k(z)\psi_0(x) + S^{kl}(z)\frac{\partial \phi^l}{\partial x}(x) \tag{4}$$

where $S^k(z), S^{kl}(z)$ are the cubic functions of z; u_{x_0} and ψ_0 are the translation and the rotation variables respectively for the k_0^{th} layer. The functions $S^k(z), S^{kl}(z)$ are so chosen that the assumed displacement field ensures the continuity of u_x and σ_{zx} at the interfaces of layers across the thickness of the laminate and also satisfies the zero shear stress condition at the bottom and top surfaces of the beam.

The displacements field may be expressed in terms of generalized displacements $\tilde{u}_1$ and $\tilde{u}_2$ as:

$$\begin{Bmatrix} u_x \\ u_z \end{Bmatrix} = \begin{bmatrix} g_1(z) & O_{1x2} \\ O_{1x4} & g_2(z) \end{bmatrix} \begin{Bmatrix} \tilde{u}_1 \\ \tilde{u}_2 \end{Bmatrix} \tag{5}$$

with

$$g_1(z) = \begin{Bmatrix} 1 & z & S^k(z) & S^{kl'}(z) \end{Bmatrix}, \qquad g_2(z) = \begin{Bmatrix} 1 & \bar{\xi}_\phi^{l'}(z) \end{Bmatrix} \tag{6}$$

$$\tilde{u}_1 = \begin{Bmatrix} u_{x_0} & -\dfrac{\partial u_{z_0}}{\partial x} & \psi_0 & \dfrac{\partial \phi^{l'}}{\partial x} \end{Bmatrix}^T, \qquad \tilde{u}_2 = \begin{Bmatrix} u_{z_0} & -\phi^{l'} \end{Bmatrix}^T \tag{7}$$

where O_{1x2} is null matrix of order 1x2 and O_{1x4} is a null matrix of order 1x4, the index $l' = 1, 2, - - -, n_\phi$. Substituting the assumed displacement field and potential field in partially nonlinear strain-displacement relations and electric field-potential relations respectively, the strains and the electric fields may be obtained as:

$$\begin{Bmatrix} \varepsilon_x \\ \gamma_{zx} \end{Bmatrix} = \begin{Bmatrix} \varepsilon_x^{(0)} \\ \gamma_{zx}^{(0)} \end{Bmatrix} + z \begin{Bmatrix} \varepsilon_x^{(1)} \\ \gamma_{zx}^{(1)} \end{Bmatrix} + S^k(z) \begin{Bmatrix} \varepsilon_x^{(2)} \\ \gamma_{zx}^{(2)} \end{Bmatrix} + S^{kl'}(z) \begin{Bmatrix} \varepsilon_x^{(3)} \\ \gamma_{zx}^{(3)} \end{Bmatrix} + \frac{\partial S^k(z)}{\partial z} \begin{Bmatrix} \varepsilon_x^{(4)} \\ \gamma_{zx}^{(4)} \end{Bmatrix} + \frac{\partial S^{kl'}(z)}{\partial z} \begin{Bmatrix} \varepsilon_x^{(5)} \\ \gamma_{zx}^{(5)} \end{Bmatrix} + \bar{\xi}_\phi^{l'}(z) \begin{Bmatrix} \varepsilon_x^{(6)} \\ \gamma_{zx}^{(6)} \end{Bmatrix} \tag{8}$$

and

$$\begin{Bmatrix} E_x \\ E_z \end{Bmatrix} = \begin{Bmatrix} E_x^{(1)} \\ E_z^{(1)} \end{Bmatrix} \xi_\phi^{l'}(z) + \begin{Bmatrix} E_x^{(2)} \\ E_z^{(2)} \end{Bmatrix} \frac{\partial \xi_\phi^{l'}(z)}{\partial z} \tag{9}$$

where the various strain components are:

$$\begin{Bmatrix} \varepsilon_x^{(0)} \\ \gamma_{zx}^{(0)} \end{Bmatrix} = \begin{Bmatrix} \dfrac{\partial u_{x0}}{\partial x} + \dfrac{1}{2}\left(\dfrac{\partial u_{z0}}{\partial x}\right)^2 \\ 0 \end{Bmatrix}, \quad \begin{Bmatrix} \varepsilon_x^{(1)} \\ \gamma_{zx}^{(1)} \end{Bmatrix} = \begin{Bmatrix} -\dfrac{\partial^2 u_{z0}}{\partial x^2} \\ 0 \end{Bmatrix}, \quad \begin{Bmatrix} \varepsilon_x^{(2)} \\ \gamma_{zx}^{(2)} \end{Bmatrix} = \begin{Bmatrix} \dfrac{\partial \psi_0}{\partial x} \\ 0 \end{Bmatrix},$$
$$\begin{Bmatrix} \varepsilon_x^{(3)} \\ \gamma_{zx}^{(3)} \end{Bmatrix} = \begin{Bmatrix} \dfrac{\partial^2 \phi^{l'}}{\partial x^2} \\ 0 \end{Bmatrix}, \quad \begin{Bmatrix} \varepsilon_x^{(4)} \\ \gamma_{zx}^{(4)} \end{Bmatrix} = \begin{Bmatrix} 0 \\ \psi_0 \end{Bmatrix}, \quad \begin{Bmatrix} \varepsilon_x^{(5)} \\ \gamma_{zx}^{(5)} \end{Bmatrix} = \begin{Bmatrix} 0 \\ \dfrac{\partial \phi^{l'}}{\partial x} \end{Bmatrix}, \quad \begin{Bmatrix} \varepsilon_x^{(6)} \\ \gamma_{zx}^{(6)} \end{Bmatrix} = \begin{Bmatrix} 0 \\ -\dfrac{\partial \phi^{l'}}{\partial x} \end{Bmatrix} \tag{10}$$

and the electric field components are:

$$\begin{Bmatrix} E_x^{(1)} \\ E_z^{(1)} \end{Bmatrix} = \begin{Bmatrix} -\dfrac{\partial \phi^{l'}}{\partial x} \\ 0 \end{Bmatrix}, \qquad \begin{Bmatrix} E_x^{(2)} \\ E_z^{(2)} \end{Bmatrix} = \begin{Bmatrix} 0 \\ -\phi^{l'} \end{Bmatrix} \tag{11}$$

The strains may also be shown in terms of the generalised beam mechanical strains $\tilde{\varepsilon}_1$ and $\tilde{\varepsilon}_5$ as:

$$\begin{Bmatrix} \varepsilon_x \\ \gamma_{zx} \end{Bmatrix} = \begin{bmatrix} g_1(z) & O_{1x2} \\ O_{1x4} & g_5(z) \end{bmatrix} \begin{Bmatrix} \tilde{\varepsilon}_1 \\ \tilde{\varepsilon}_5 \end{Bmatrix} + \begin{Bmatrix} 1/2\left(\dfrac{\partial u_{z0}}{\partial x}\right)^2 \\ 0 \end{Bmatrix} \tag{12}$$

where $\tilde{\varepsilon}_1$ and $\tilde{\varepsilon}_5$ are given by:

$$\tilde{\varepsilon}_1 = \begin{Bmatrix} \dfrac{\partial u_{x0}}{\partial x} & -\dfrac{\partial^2 u_{z0}}{\partial x^2} & \dfrac{\partial \psi_0}{\partial x} & \dfrac{\partial^2 \phi^l}{\partial x^2} \end{Bmatrix}^T, \qquad \tilde{\varepsilon}_5 = \begin{Bmatrix} \psi_0 & \dfrac{\partial \phi^l}{\partial x} \end{Bmatrix}^T \tag{13}$$

and the vector $g_5(z)$ is defined as

$$g_5(z)=\left\{\frac{\partial S^k(z)}{\partial z} \quad \left(\frac{\partial S^{kl}(z)}{\partial z}-\bar{\xi}_\phi^l(z)\right)\right\} \tag{14}$$

The variational equation for the beam is obtained as:

$$\int_0^a \left[\begin{array}{l} \delta\tilde{\varepsilon}_1^T F_1+\delta\tilde{\varepsilon}_5^T F_5+\left\{\frac{\partial\delta\phi^l}{\partial x} \quad \delta\phi^l\right\}\left\{H^l \quad G^l\right\}^T \\ -\delta\tilde{u}_2^T\left\{q_2 \quad -q_4^l\right\}^T+\left(\frac{\partial\delta u_{z_0}}{\partial x}N_x\frac{\partial u_{z_0}}{\partial x}\right) \end{array}\right]dx$$
$$-\left[N_x^*\delta u_{x_0}^*+V_x^*\delta u_{z_0}^*-M_x^*\frac{\partial\delta u_{z_0}^*}{\partial x}+P_x^*\delta\psi_0^*+\left(H^{l*}-V_\phi^{l*}\right)\delta\phi^{l*}+R_x^{l*}\frac{\partial\delta\phi^{l*}}{\partial x}\right]_0^a=0 \tag{15}$$

where the superscript * means values at the ends. F_1, F_5, V_x and V_ϕ^l are the beam stress resultants given by:

$$F_1=\sum_{k=1}^{N}\int_{z_{k-1}}^{z_k}\left\{\begin{array}{c}1\\ z\\ S^k(z)\\ S^{kl}(z)\end{array}\right\}\sigma_x^{(k)}bdz\,, \qquad F_5=\sum_{k=1}^{N}\int_{z_{k-1}}^{z_k}\left\{\begin{array}{c}\frac{\partial S^k(z)}{\partial z}\\ \left(\frac{\partial S^{kl}(z)}{\partial z}-\bar{\xi}_\phi^l(z)\right)\end{array}\right\}\sigma_{zx}^{(k)}bdz \tag{16}$$

$$V_x=\sum_{k=1}^{N}\int_{z_{k-1}}^{z_k}\sigma_{zx}^{(k)}bdz\,, \qquad V_\phi^l=\sum_{k=1}^{N}\int_{z_{k-1}}^{z_k}\bar{\xi}_\phi^l(z)\sigma_{zx}^{(k)}bdz \tag{17}$$

and H^l and G^l are the beam electric displacement resultants given by:

$$H^l=\sum_{k=1}^{N}\int_{z_{k-1}}^{z_k}D_x^{(k)}\xi_\phi^l(z)bdz\,, \qquad G^l=\sum_{k=1}^{N}\int_{z_{k-1}}^{z_k}D_z^{(k)}\frac{\partial\xi_\phi^l(z)}{\partial z}bdz \tag{18}$$

q_2 and q_4^l are the mechanical load and electrical load respectively.

3 FINITE ELEMENT MODEL

A one dimensional finite element model (1D-FE) based on efficient layerwise (zigzag) theory is used for the analysis. Two noded elements (Kapuria et al., 2004) are considered for the electromechanical variables (Figure 2). The 1D beam element has eight mechanical and a variable number of electrical degrees of freedom.

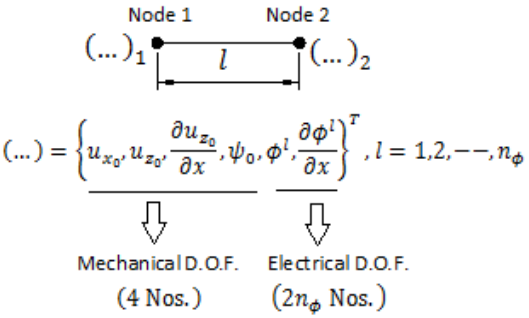

Figure 2: *Two noded 1D beam element with degrees of freedom*

The highest order of the derivatives of the variables u_{z_0} and ϕ^l, in the variational Eq. (15) when expanded in terms of the primary variables (u_{x_0}, u_{z_0}, ψ_0 and ϕ^l), is 2 and that of the other two variables u_{x_0} and ψ_0 is 1. Therefore, in order to satisfy the convergence requirements of the finite element procedure $u_{x_0}, \frac{\partial u_{z_0}}{\partial x}, \psi_0$ and $\frac{\partial \phi^l}{\partial x}$ are required to be continuous at the boundaries of the element considered. Hence cubic Hermite interpolation (Kapuria et al., 2004) is used for expanding u_{z_0} and ϕ^l whereas u_{x_0} and ψ_0 are expanded using linear Lagrange interpolation.

$$\begin{Bmatrix} u_{x_0} \\ u_{z_0} \\ \psi_0 \\ \phi^l \end{Bmatrix} = \begin{bmatrix} \tilde{N} & 0 & 0 & 0 \\ 0 & \hat{N} & 0 & 0 \\ 0 & 0 & \tilde{N} & 0 \\ 0 & 0 & 0 & \hat{N} \end{bmatrix} \begin{Bmatrix} u_{x_0}^e \\ u_{z_0}^e \\ \psi_0^e \\ \phi^{l^e} \end{Bmatrix} \tag{19}$$

where $\tilde{N}$ and $\hat{N}$ are vectors of linear interpolation functions and cubic Hermite interpolation functions respectively; $u_{x_0}^e, u_{z_0}^e, \psi_0^e$ and ϕ^{l^e} are the nodal value vectors.

The integrand in the variational Eq. (15) may be shown as

$$\delta\bar{\varepsilon}^T \bar{F} - \delta\tilde{u}_2^T g_{u\phi} + \left(\frac{\partial \delta u_{z_0}}{\partial x} N_x \frac{\partial u_{z_0}}{\partial x} \right) \tag{20}$$

where $\bar{F}$ is the generalised stress vector, $\bar{\varepsilon}$ is the generalised strains vector and $g_{u\phi}$ is the electromechanical load vector of the beam defined as

$$\bar{F} = \left\{ F_1^T \quad F_5^T \quad H^l \quad G^l \right\}^T, \qquad \bar{\varepsilon} = \left\{ \tilde{\varepsilon}_1^T \quad \tilde{\varepsilon}_5^T \quad \frac{\partial \phi^l}{\partial x} \quad \phi^l \right\}^T, \qquad g_{u\phi} = \left\{ q_2 \quad -q_4^l \right\}^T \tag{21}$$

Substituting for $\bar{F}$ and N_x, the participation in T^e of one element to the integral from 0 to l in Eq. (15) is attained as

$$T^e = \int_0^l \left[\begin{array}{l} \delta\bar{\varepsilon}^T \left(\bar{D}\bar{\varepsilon} + \frac{1}{2} g_n \left(\frac{\partial u_{z_0}}{\partial x} \right)^2 \right) - \delta\tilde{u}_2^T g_{u\phi} \\ + \frac{\partial \delta u_{z_0}}{\partial x} \left(A_1^T \tilde{\varepsilon}_1 + \beta_1^{l'} \phi^{l'} + \frac{1}{2} A_{11} \left(\frac{\partial u_{z_0}}{\partial x} \right)^2 \right) \frac{\partial u_{z_0}}{\partial x} \end{array} \right] dx \tag{22}$$

where $\bar{D}$ is the generalised stiffness matrix, g_n is the matrix that relates $\bar{F}$ with nonlinear strain and A_1 is the first column of beam stiffness matrix A.

Assuming small displacements and strains and considering linear elastic behavior, the nonlinear terms are ignored. Thus Eq. (22) may be simplified for linear analysis as

$$T^e = \int_0^l \left[\delta\bar{\varepsilon}^T \bar{D}\bar{\varepsilon} - \delta\tilde{u}_2^T g_{u\phi} \right] dx \tag{23}$$

The generalised displacement vector, d^e for the element is defined as

$$d^{e^T} = \left\{ u_{x_0}^{e^T} \quad u_{z_0}^{e^T} \quad \psi_0^{e^T} \quad \phi^{l^{e^T}} \right\} \tag{24}$$

Using Eqs. (7), (13), (21) and (24), the generalised displacements $\tilde{u}_2$ and strains $\bar{\varepsilon}$ can be expressed in terms of d^e as

$$\tilde{u}_2 = \bar{B}_{m_2} d^e, \qquad \bar{\varepsilon} = \bar{B} d^e \tag{25}$$

where $\bar{B}_{m_2}$ and $\bar{B}$ are displacement interpolation and strain displacement matrices. Using Eq. (25) for $\tilde{u}_2$ and $\bar{\varepsilon}$ in Eq. (23), T^e may be shown as

$$\begin{aligned} T^e &= \int_0^l \delta d^{eT} \left[\bar{B}^T \bar{D} \bar{B} d^e - \bar{B}_{m_2}^T g_{u\phi} \right] dx \\ &= \delta d^{eT} \left[K^e d^e - P^e \right] \end{aligned} \tag{26}$$

with

$$K^e = \int_0^l \bar{B}^T \bar{D} \bar{B} dx, \qquad P^e = \int_0^l \bar{B}_{m_2}^T g_{u\phi} dx \tag{27}$$

The contributions from all the elements are summed up to obtain the system equation as

$$Kd = P \tag{28}$$

in which K is the assembled stiffness matrix and d and P are the assembled displacement and load vectors respectively. The boundary conditions for clamped end and free end are

$$\begin{aligned} &\text{Clamped end: } u_{x_0} = 0,\ u_{z_0} = 0,\ \frac{\partial u_{z_0}}{\partial x} = 0,\ \psi_0 = 0, \\ &\text{Free end: } \quad N_x = 0,\ V_x = 0,\ M_x = 0,\ P_x = 0. \end{aligned} \tag{29}$$

The beam is modelled with separate segments for elastic parts and hybrid parts. The hybrid parts have PZT-5A patch bonded on the top surface of the elastic substrate whereas the elastic parts are without piezoelectric patch. The elastic parts have four numbers of nodal electric degrees of freedom however hybrid parts have 12, as four sub-layers are considered through the thickness of the piezoelectric layer.

To show the accuracy and efficiency of the present formulation, the results of 1D-FE model are compared with the converged 2D-FE (ABAQUS) results (Khan et al., 2016). The hybrid beams are modelled in 2D planar modelling space as a deformable shell using FE package ABAQUS (2010) wherein the layup with different material properties are defined across the beam thickness and suitable element types for elastic substrate and piezoelectric layers are assigned. The thickness direction is also discretised for displacements. An 8-noded biquadratic plane stress piezoelectric quadrilateral element is used for piezo layers and an 8-noded biquadratic plane stress quadrilateral element with reduced integration is used for the elastic layers of hybrid beams for generating the finite element mesh in ABAQUS. The geometric order is considered linear for both type of elements.

4 RESULTS AND DISCUSSIONS

4.1 Validation

The 1D-FE formulation is first validated by considering the flexural analysis problem (Problem 2) of Ganapathi et al. (2004) for a piezoelectric sandwich beam. Mechanical and potential load cases are considered for the problem beam with cantilever end conditions. A point load of 1 N is applied, at the free end, for the former whereas for latter an electric potential (100 V) is applied at the top/bottom surfaces. The geometrical configuration of beam and the properties of the material are taken from Ganapathi et al. (2004). The results are compared (Table 1) for span to thickness ratio $S(=l/h)=10$. The %age of difference of the present 1D-FE results with respect to the results presented in Ganapathi et al. (2004) is in a range of 2.5% - 2.8% for the case of mechanical load and 3.3% - 8.6% for the case of potential load.

Table 1: *Comparison of 1D-FE results for cantilever piezoelectric sandwich beam with Ganapathi et al. (2004).*

			Mechanical load case		Potential load case	
S. No.	Entity	Units	1D-FE	Ganapathi et al. (2004)*	1D-FE	Ganapathi et al. (2004)*
1	$10^7 u_z(0.2,-0.05)$	m	1.50	1.54	-3.17	-2.92
2	$10^7 u_x(0.2,-0.05)$	m	0.72	0.70	-1.45	-1.50
3	$\sigma_x(0.2,-0.05)$	N/m^2	23164	23750	-5410	-6000

* Results read from graphs

4.2 Numerical Example

To assess the effect of size and position of piezoelectric patch on static response of a smart beam, two beam configurations, (b) and (c) are considered. The substrate (b) is a four layers symmetric graphite epoxy composite laminate with layup (0^o, 90^o, 90^o, 0^o). The thickness of each layer of the composite laminate is taken as $0.25h$, where h is the total thickness of elastic substrate at any section. The substrate (c) is a three layers symmetric sandwich with top and bottom face sheets of thicknesses $0.08h$ and an in-between soft core of thickness $0.84h$. The total thickness of elastic substrate at any section remains the same. Piezoelectric patches (PZT-5A) of variable size are bonded on the top surfaces of the elastic substrate at varied axial locations. The thickness of piezo-patches is taken as $0.1h$. The PZT-5A patches have polling in +z direction. The top and bottom surfaces of the elastic substrate are grounded. The properties of the materials used are listed in Table 2 (Rahman and Alam, 2015).

The following load cases are considered

(1) A uniform pressure $q_t = -q_0$ on the top surface over entire length with open circuit condition.

(2) A uniform pressure $q_t = -q_0$ on the top surface over entire length with closed circuit condition.

(3) A uniform applied potential $\phi^{n\phi} = -\phi_0$ on the top surface of the piezoelectric patch layer.

Table 2: *Material properties for substrates (b) and (c).*

Material	Y_1	Y_2	Y_3	G_{12}	G_{23}	G_{13}	ν_{12}	ν_{13}	ν_{23}	ρ
			GPa							kgm^{-3}
Graphite epoxy	181	10.3	10.3	7.17	2.87	7.17	0.28	0.28	0.33	1578
Face	131.1	6.9	6.9	3.588	2.3322	3.588	0.32	0.32	0.49	1000
Core	22.08 x 10^{-5}	20.01 x 10^{-5}	2.76	0.01656	0.4554	0.5451	0.99	3 x 10^{-5}	3 x10^{-5}	70
PZT-5A	61	61	53.2	22.6	21.1	21.1	0.35	0.38	0.38	7600

	d_{31}	d_{32}	d_{33}	d_{15}	d_{24}	η_{11}	η_{22}	η_{33}
PZT-5A		(x 10^{-12} mV^{-1})				(x 10^{-8} Fm^{-1})		
	-171	-171	374	584	584	1.53	1.53	1.5

The non-dimensionalised results are obtained as:

1) $\bar{u}_z = 100u_z Y_0 / hS^4 q_0$, $\bar{u}_x = 100u_x Y_0 / hS^3 q_0$, $\bar{\sigma}_x = \sigma_x / S^2 q_0$, $\bar{\phi} = 10^4 \phi Y_0 d_0 / hS^2 q_0$

2) $\hat{u}_z = 10u_z / S^2 d_0 \phi_0$, $\hat{u}_x = 10u_x / S d_0 \phi_0$, $\hat{\sigma}_x = \sigma_x h / 10 Y_0 d_0 \phi_0$

where $S = l/h$ is the span to thickness ratio, Y_0 for beam (b) is taken as $10.3GPa$ and for beam (c) $6.9GPa$. d_0 is taken as 374 x 10^{-12} CN^{-1}.

4.2.1 Static response with variation of piezo-patch layer position

Cantilever beams (b) and (c), with a piezoelectric patch of length $0.4l$, bonded on top of the elastic substrate at a distance x_p from the fixed end (Figure 3) are considered for the analysis. The beams are modelled and analyzed with different values of x_p.

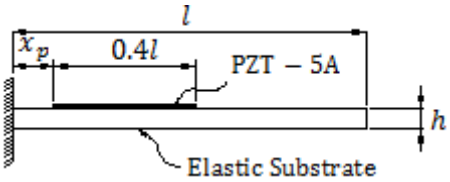

Figure 3: *Cantilever beam with piezoelectric patch layer at variable position.*

The deflection profile of centrelines are compared in Figure 4 under load case 3. Here the mid-surface deflection is more for piezo-patch positions nearer to the fixed end. Therefore, the piezoelectric patch actuators should be placed nearer to the fixed end for control of tip deflection in cantilever beams. However, the tip deflection is more as the piezo-patch position is moved farther from the fixed end of cantilever beam for pressure load cases 1 and 2 (Figure 5). This is due to increased bending moment resulting from larger distance of piezo-patch from the fixed end. The axial displacement and normal stress distribution across the thickness at mid position of piezoelectric patch are compared in Figure 6 for beams (b) and (c).

Figure 7 shows comparison of through the thickness distribution of axial displacement and normal stress at the centre of the piezoelectric patch for pressure load case 2 and potential load case 3.The maximum normal stress occur in load case 3.

The through the thickness distribution profiles of axial displacement and normal stresses at mid position of piezoelectric patch for pressure load cases show increasing trend for u_x and decreasing trend for σ_x with increase in distance of piezo-patch from the fixed end. However for load case 3 no significant variation is observed for the axial displacement at the top surface of piezoelectric patch and normal stress at the bottom surface of piezoelectric patch with variation in piezo-patch positions from the fixed end. These observations are clearer in Figure 8, showing variation of these parameters with position of piezo-patch layer.

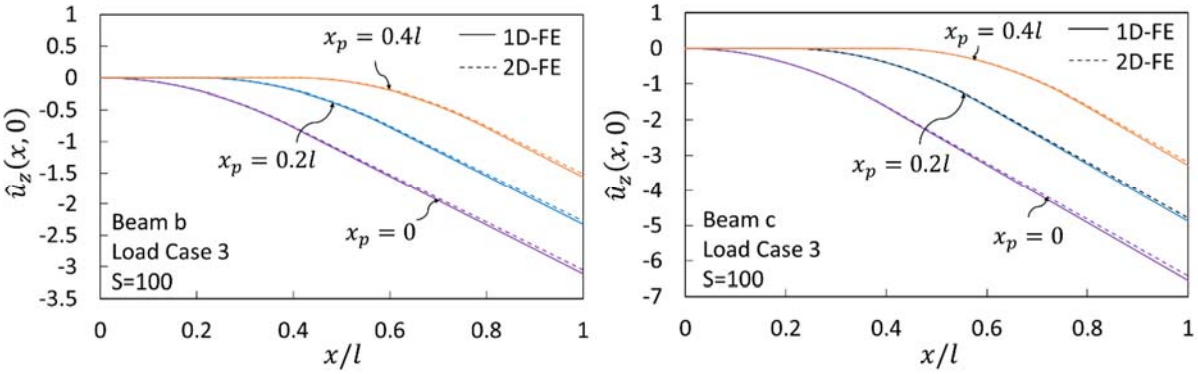

Figure 4: *Deflection profile of centre lines of cantilever beams for various piezo patch positions.*

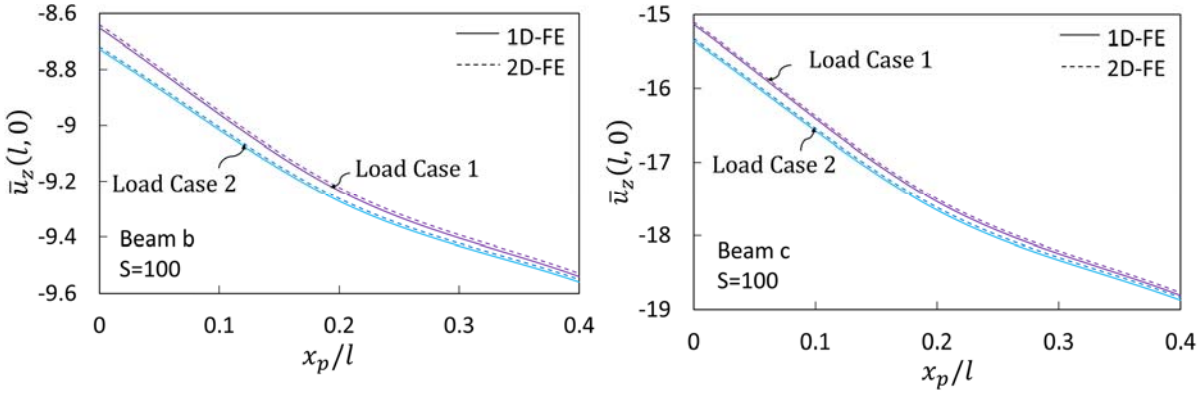

Figure 5: *Variation of tip deflection of cantilever beam with piezo patch position.*

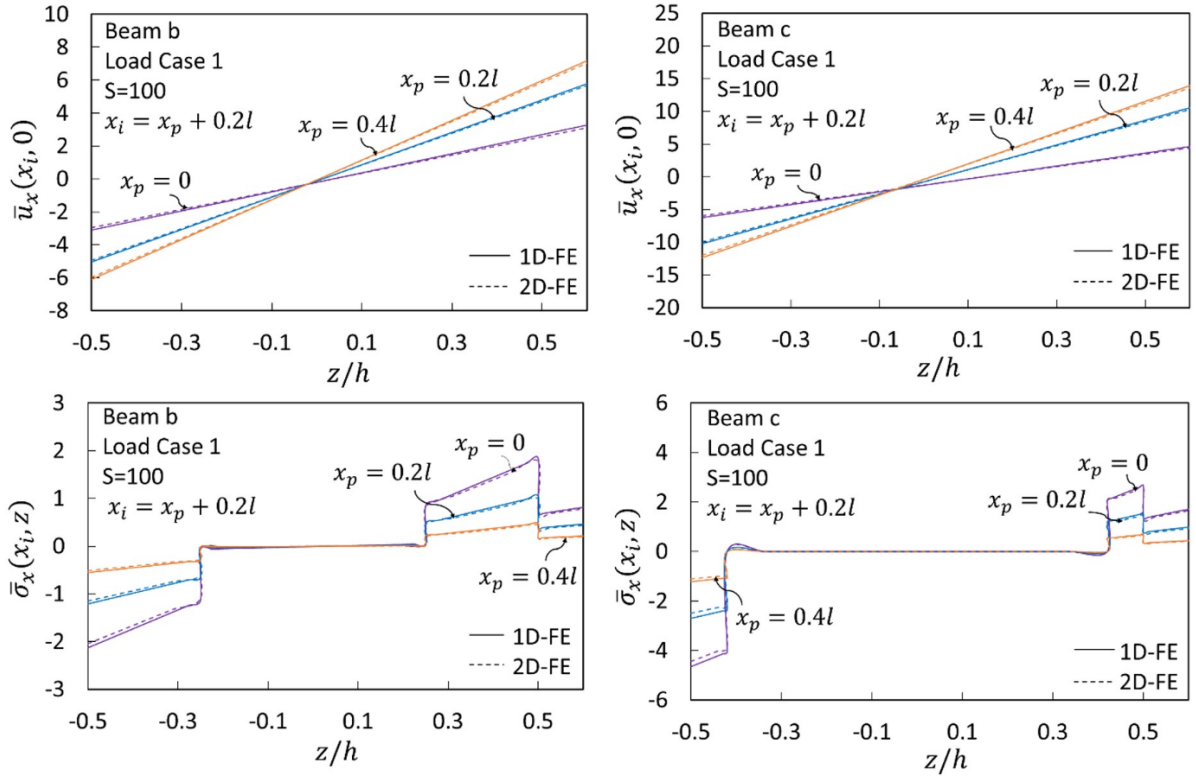

Figure 6: *Through the thickness distribution of axial displacement and normal stress at the centre of piezoelectric patch for various patch positions.*

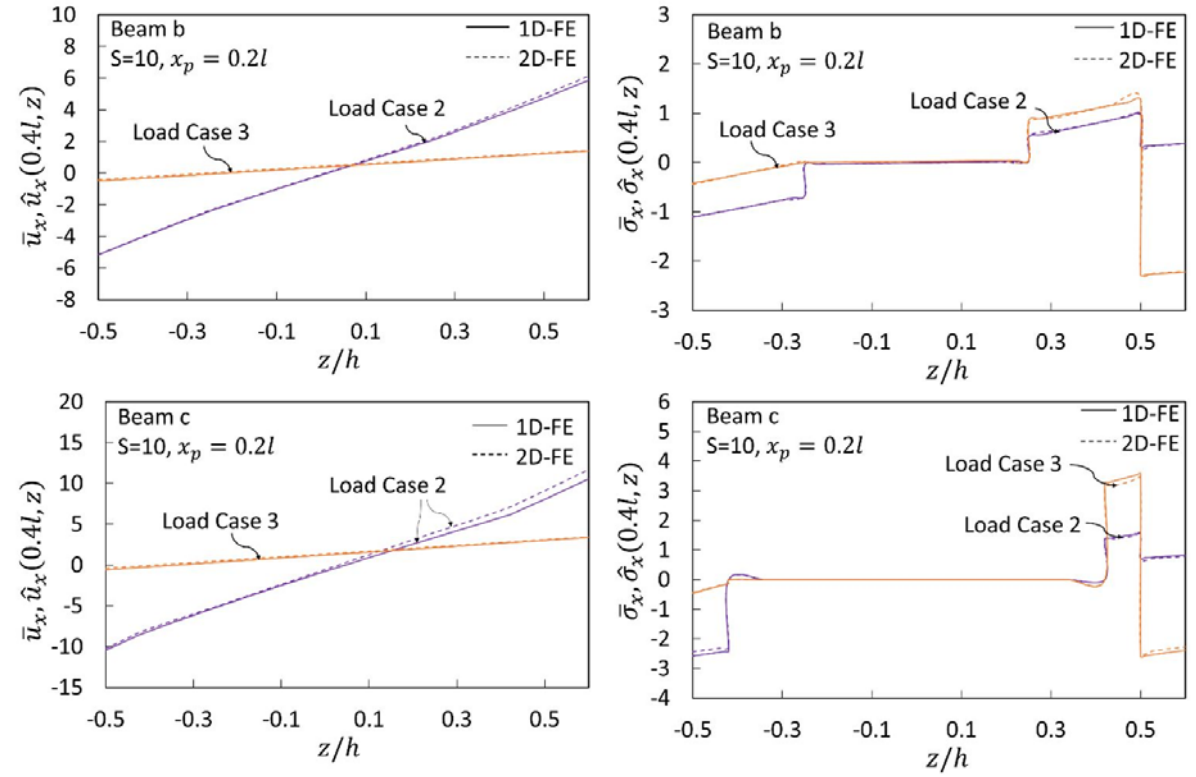

Figure 7: *Comparison of axial displacement and normal stress across the thickness in beams (b) and (c).*

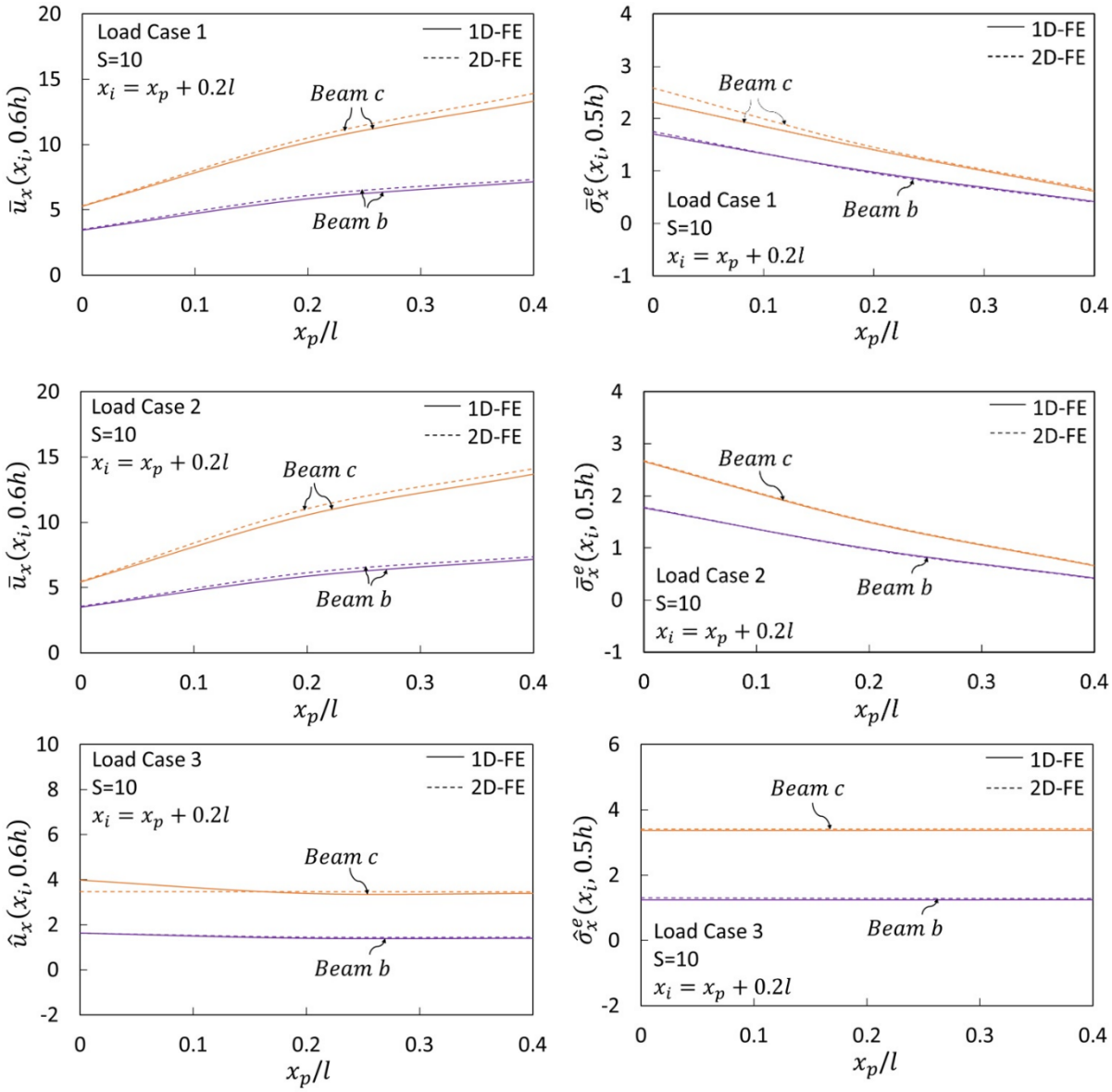

Figure 8: *Variation of axial displacement and normal stress with position of piezo-patch layer.*

Tables 3 and 4 show the mid-surface deflection at the free end, the axial displacement and normal stress at the centre of piezoelectric patch layer $(x = x_p + 0.2l)$ for beams (b) and (c) respectively. The results are presented in non-dimensional form but the bar and hat are omitted. The two results are in good agreement with each other.

Table 3: *Comparison of 1D-FE and 2D-FE results for beam (b) with variation of piezo-patch position.*

			Load case 1		Load case 2		Load case 3	
S	x_p	Entity	1D-FE	2D-FE	1D-FE	2D-FE	1D-FE	2D-FE
10	0	$u_z(l,0)$	-10.191	-10.191	-10.274	-10.268	-3.031	-3.006
		$u_x(0.2l,0.6h)$	3.450	3.520	3.504	3.568	1.635	1.626
		$\sigma_x(0.2l,-0.5h)$	-1.990	-2.010	-2.006	-2.015	-0.416	-0.434
		$\sigma_x^e(0.2l,0.5h)$	1.710	1.750	1.771	1.779	1.269	1.301
		$\sigma_x(0.2l,0.6h)$	0.770	0.760	0.714	0.715	-2.221	-2.205
	$0.2l$	$u_z(l,0)$	-10.730	-10.901	-10.770	-10.963	-2.067	-2.029
		$u_x(0.4l,0.6h)$	5.850	6.110	5.876	6.140	1.399	1.443
		$\sigma_x(0.4l,-0.5h)$	-1.080	-1.090	-1.105	-1.099	-0.418	-0.443
		$\sigma_x^e(0.4l,0.5h)$	0.980	0.960	0.984	0.971	1.269	1.289
		$\sigma_x(0.4l,0.6h)$	0.420	0.410	0.389	0.380	-2.221	-2.215
	$0.4l$	$u_z(l,0)$	-11.071	-11.230	-11.088	-11.242	-1.378	-1.352
		$u_x(0.6l,0.6h)$	7.151	7.340	7.167	7.358	1.399	1.443
		$\sigma_x(0.6l,-0.5h)$	-0.450	-0.460	-0.462	-0.461	-0.417	-0.438
		$\sigma_x^e(0.6l,0.5h)$	0.420	0.410	0.423	0.413	1.269	1.287
		$\sigma_x(0.6l,0.6h)$	0.170	0.160	0.158	0.150	-2.221	-2.215

Table 4: *Comparison of 1D-FE and 2D-FE results for beam (c) with variation of piezo-patch position.*

			Load case 1		Load case 2		Load case 3	
S	x_p	Entity	1D-FE	2D-FE	1D-FE	2D-FE	1D-FE	2D-FE
10	0	$u_z(l,0)$	-20.754	-20.66	-20.754	-20.874	-6.265	-6.338
		$u_x(0.2l,0.6h)$	5.283	5.311	5.434	5.473	3.983	3.475
		$\sigma_x(0.2l,-0.5h)$	-4.899	-4.365	-4.410	-4.377	-0.437	-0.443
		$\sigma_x^e(0.2l,0.5h)$	2.219	2.586	2.661	2.681	3.400	3.401
		$\sigma_x(0.2l,0.6h)$	1.421	1.548	1.481	1.484	-2.276	-2.254
	$0.2l$	$u_z(l,0)$	-23.748	-24.093	-23.799	-24.157	-4.211	-4.221
		$u_x(0.4l,0.6h)$	10.183	11.630	10.565	11.693	3.394	3.474
		$\sigma_x(0.4l,-0.5h)$	-2.486	-2.418	-2.454	-2.425	-0.438	-0.445
		$\sigma_x^e(0.4l,0.5h)$	1.408	1.454	1.493	1.506	3.400	3.401
		$\sigma_x(0.4l,0.6h)$	0.812	0.819	0.785	0.785	-2.274	-2.269
	$0.4l$	$u_z(l,0)$	-24.876	-25.142	-24.856	-25.161	-2.828	-2.814
		$u_x(0.6l,0.6h)$	13.320	14.454	13.686	14.485	3.394	3.463
		$\sigma_x(0.6l,-0.5h)$	-1.077	-1.034	-1.055	-1.037	-0.438	-0.442
		$\sigma_x^e(0.6l,0.5h)$	0.617	0.646	0.659	0.668	3.400	3.402
		$\sigma_x(0.6l,0.6h)$	0.301	0.302	0.291	0.288	-2.275	-2.261

4.2.2 Static response with variation of size of piezo-patch layer

Cantilever beams with a piezoelectric patch of length l_p, bonded on top of the elastic substrate at the fixed end (Figure 9) are considered for the analysis. The beams are modelled and analysed for load case 3, with different values of l_p for graphite epoxy composite substrate (b) and sandwich substrate (c). The width of the beam and piezo patch are modelled as unity.

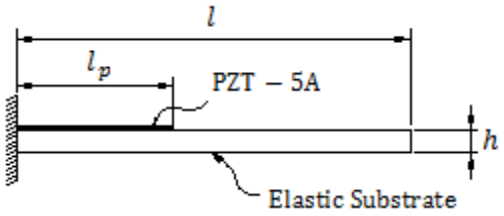

Figure 9: *Cantilever beam with a piezoelectric patch layer of variable size.*

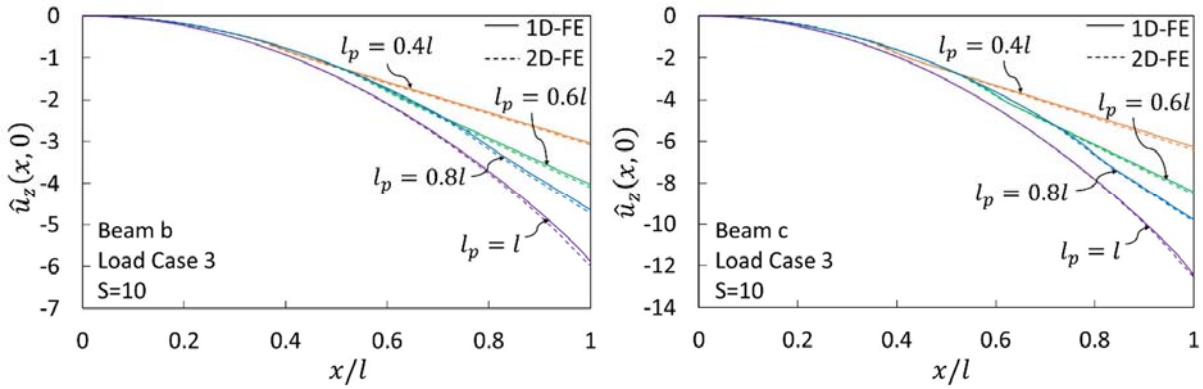

Figure 10: *Deflection profile of centre lines of cantilever beams for various piezo patch lengths.*

The deflection profiles of centreline are compared in Figure 10. The centre line deflection is more as the piezo-patch size is increased. Figure 11 shows variation of mid surface deflection at the free end and axial displacement at the top of the elastic substrate at the free end, with size of piezoelectric layer. The absolute numerical value of both these parameters reflect an increasing trend.

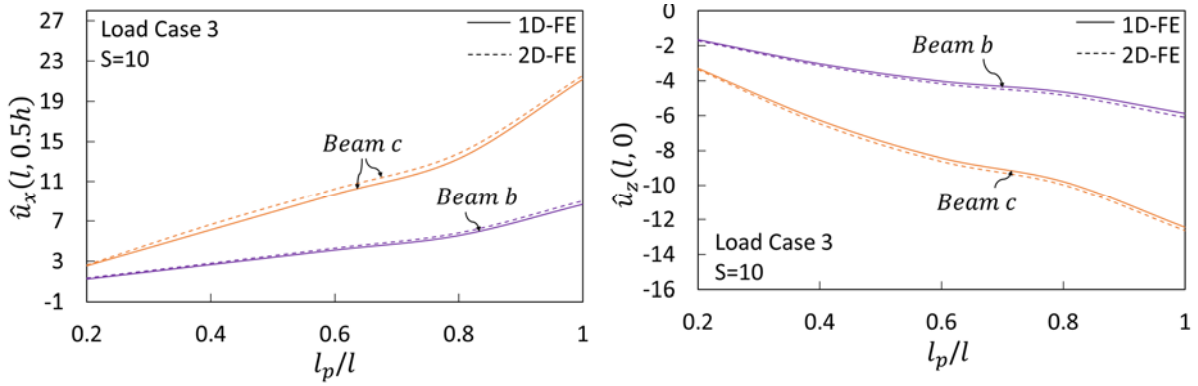

Figure 11: *Variation of axial and transverse displacements with size of piezo-patch layer.*

The mid-surface deflection at the free end, the axial displacement and the normal stress at the center of piezoelectric patch $(x = l_p / 2)$ are presented in Table 5 for beams (b) and (c). The results are in good agreement with the 2D-FE results obtained using ABAQUS for both the beams.

Table 5: *Comparison of 1D-FE and 2D-FE results with variation of piezo-patch size.*

			Beam b		Beam c	
S	l_p	Entity	1D-FE	2D-FE	1D-FE	2D-FE
10	$0.4l$	$u_z(l,0)$	-3.031	-3.006	-6.265	-6.338
		$u_x(0.2l,0.6h)$	1.635	1.626	3.983	3.956
		$\sigma_x(0.2l,-0.5h)$	-0.417	-0.430	-0.437	-0.441
		$\sigma_x^e(0.2l,0.5h)$	1.268	1.286	3.400	3.402
		$\sigma_x(0.2l,0.6h)$	-2.221	-2.214	-2.276	-2.273
	$0.6l$	$u_z(l,0)$	-4.028	-4.010	-8.430	-8.462
		$u_x(0.3l,0.6h)$	2.453	2.438	5.974	5.947
		$\sigma_x(0.3l,-0.5h)$	-0.416	-0.418	-0.437	-0.437
		$\sigma_x^e(0.3l,0.5h)$	1.268	1.270	3.400	3.400
		$\sigma_x(0.3l,0.6h)$	-2.222	-2.220	-2.276	-2.274
	$0.8l$	$u_z(l,0)$	-4.642	-4.630	-9.788	-9.778
		$u_x(0.4l,0.6h)$	3.270	3.254	7.966	7.938
		$\sigma_x(0.4l,-0.5h)$	-0.416	-0.416	-0.437	-0.437
		$\sigma_x^e(0.4l,0.5h)$	1.268	1.268	3.400	3.400
		$\sigma_x(0.4l,0.6h)$	-2.222	-2.221	-2.276	-2.274
	l	$u_z(l,0)$	-5.875	-5.864	-12.442	-12.389
		$u_x(0.5l,0.6h)$	4.497	4.479	10.953	10.924
		$\sigma_x(0.5l,-0.5h)$	-0.457	-0.457	-0.480	-0.480
		$\sigma_x^e(0.5l,0.5h)$	1.395	1.395	3.740	3.740
		$\sigma_x(0.5l,0.6h)$	-2.440	-2.441	-2.503	-2.501

4.2.3 Shape control using piezoelectric patches

The problem beams are further analyzed for electromechanical load case (load case 4), where a pressure $q_t = q_0$ is applied on the top surface over entire length with uniform applied potential $\phi^{n\phi} = \phi_0$ on the top surface of the piezoelectric patch layer. Keeping the pressure as same, the applied potential is increased to reduce the centre line deflection. The results are obtained with lengths of piezoelectric patch, $l_p = 0.4l, 0.6l$. As the size of the patch increases, the value of the applied potential, required to minimise the tip deflection, decreases. But at the same time the curvature of the deflected beam also increases for the portion where piezoelectric patch is bonded on the top surface (Figure 12). This shows that a single piezo patch is not suitable for controlling the deflected shape of beam. The problem may be overcome by using multiple piezoelectric patches with different applied voltages on each. Figure 13 shows the shape control for beam (b) having four numbers of piezoelectric patches bonded on top surface of the beam. Their positions (x_1, x_2, x_3, x_4), sizes (l_1, l_2, l_3, l_4) and the applied voltages $\left(\bar{\phi}_1, \bar{\phi}_2, \bar{\phi}_3, \bar{\phi}_4\right)$ are mentioned in the figure.

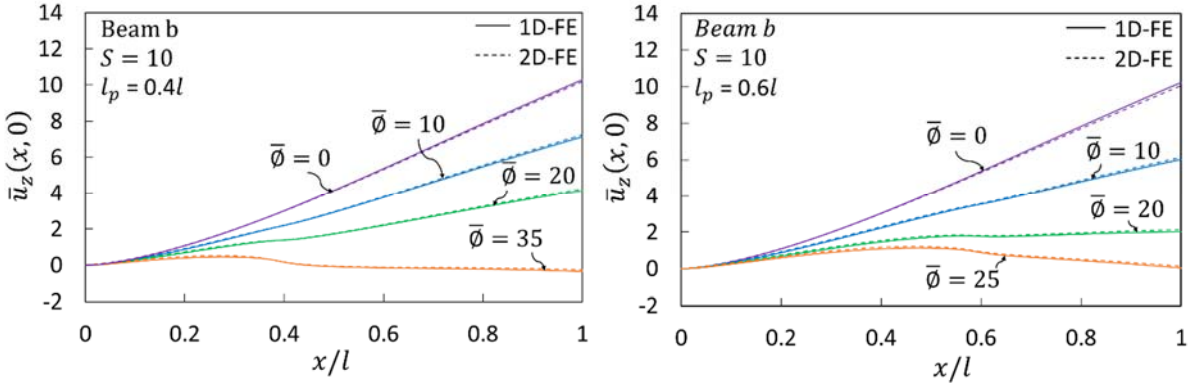

Figure 12: *Deflection profile of centre line with variation of size of piezo-patch layer for load case 4.*

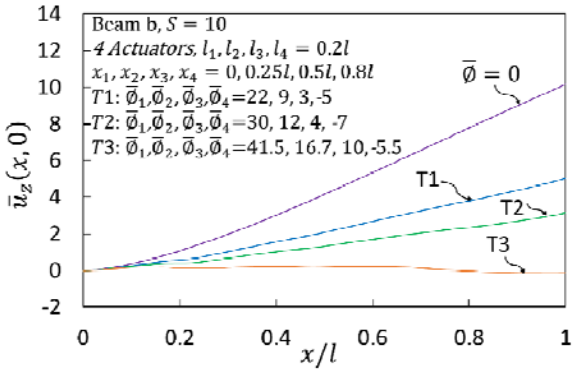

Figure 13: *Shape control for beam (b) with four numbers of piezo patches bonded on top surface of the beam.*

The excellent agreement with the 2D-FE (ABAQUS) results proves the accuracy of the present 1D-FE formulation based on efficient zigzag theory. Furthermore, the advantage of using present formulation is the smaller problem size in comparison to the 2D-FE (ABAQUS) model for the same computational accuracy. As the beam thickness is also discretised in the 2D-FE (ABAQUS) model, it leads to quite large numbers of degrees of freedom in comparison to the present 1D-FE model. For example beam b, with $l_p = 0.2l$ and S=10, has been discretised into 704 elements for 2D-FE analysis as against only 40 elements in the present 1D-FE formulation. The mesh seeds and hence the total degrees of freedom increase further with beam length and number of layers across the thickness to accommodate the higher aspect ratio and material heterogeneity. The computational time taken for 2D-FE static analysis of the problem beam is about 10 times that of 1D-FE analysis. This shows the efficiency and accuracy of the present 1D-FE model.

5 CONCLUSIONS

In smart beam structures, piezoelectric layers often form an integral part of the structure owing to their ability to transform electrical energy to mechanical energy and vice versa. The location and size of these layers is significant as it results in different structural response under various loading conditions. The effect of position and size of piezoelectric layer on static response of a hybrid beam is assessed using a 1D FE model based on efficient layerwise (zigzag) theory. The results are obtained for cantilever (clamped-free) end conditions. The accuracy and efficiency of the present 1D FE model has been established by comparing the results with the 2D FE model developed in ABAQUS. The centre line deflection is more as the piezo-patch position is moved farther from the fixed end of cantilever beam for pressure load cases. The inverse is true for potential load case. Therefore, the piezoelectric patch actuators should be placed nearer to the fixed end for control of tip deflection in cantilever beam. The centre line deflection is more as the piezo-patch size is increased in potential load case. Single piezo patch is not suitable for controlling the deflected shape of beam. Using multiple piezo-patches, with different applied voltages on each, is more feasible for shape control of beam in an electromechanical load case. These observations may be used as a benchmark for experimental investigation and design for composite and sandwich hybrid structures.

References

ABAQUS. (2010). Standard User's Manual, Version 6.10, Vol. 1.

Batra R.C. and Vidoli S. (2002) Higher-order piezoelectric plate theory derived from a three-dimensional variational principle, AIAA Journal 40:91–104.

Benjeddou A. (2000) Advances in piezoelectric finite element modeling of adaptive structural elements: a survey, Computers & Structures 76:347–363.

Catapano A., Giunta G., Belouettar S., Carrera E. (2011) Static analysis of laminated beams via a unified formulation, Composite Structures 94:75–83.

Correia V.M.F., Gomes, M.A.A., Suleman A., Soares C.M.M. (2000) Modelling and design of adaptive composite structures, Computational Methods in Applied Mechanics and Engineering 185:325–346.

Filippi M., Pagani A., Petrolo M., Colonna G., Carrera E. (2015) Static and free vibration analysis of laminated beams by refined theory based on Chebyshev polynomials, Composite Structures 132:1248–1259.

Fukunaga H., Hu N., Ren G.X. (2001) FEM modeling of adaptive composite structures using a reduced higher-order plate theory via penalty functions, International Journal of Solids and Structures 38:8735–8752.

Ganapathi M., Patel B. P., Touratier M. (2004) A C1 finite element for flexural and torsional analysis of rectangular piezoelectric laminated/sandwich composite beams, International Journal of Numerical Methods in Engineering 61:584–610.

Giunta G., Belouettar S., Ferreira A.J.M. (2016) A static analysis of three-dimensional functionally graded beams by hierarchical modelling and a collocation meshless solution method, Acta Mechanica 227: 969–991.

Kapuria S. and Hagedorn P. (2007) Unified efficient layerwise theory for smart beams with segmented extension/shear mode, piezoelectric actuators and sensors, Journal of Mechanics of Materials and Structures 2:1267-1298.

Kapuria S., Dumir P.C., Ahmed A. (2003) An efficient coupled layerwise theory for static analysis of piezoelectric sandwich beams, Archive of Applied Mechanics 73:147-159.

Kapuria S., Dumir P.C., Ahmed A., Alam M.N. (2004) Finite element model of efficient zigzag theory for static analysis of hybrid piezoelectric beams, Computational Mechanics 34:475-483.

Kapuria S., Kulkarni S.D. (2008) An efficient quadrilateral element based on improved zigzag theory for dynamic analysis of hybrid plates with electroded piezoelectric actuators and sensors, J. of Sound and Vibration 315:118–145.

Khan A.A., Alam M.N., Rahman N. and Wajid M. (2016) Finite element modelling for static and free vibration response of functionally graded beam, Latin American Journal of Solids and Structures 13(4): 690-714.

Komeili A., Akbarzadeh A.H., Doroushi A. and Eslami M.R. (2011) Static Analysis of Functionally Graded Piezoelectric Beams under Thermo-Electro-Mechanical Loads, Advances in Mechanical Engineering, Article ID 153731, 10 pages. doi:10.1155/2011/153731.

Mitchell J.A., Reddy J.N. (1995) A refined hybrid plate theory for composite laminates with piezoelectric laminae, International Journal of Solids and Structures 32:2345–2367.

Rahman N., Alam M.N. (2012) Dynamic Analysis of Laminated Smart Beams using Zigzag Theory, International Journal of Mechanics Structural 3:35-46.

Rahman N., Alam M.N. (2014) Finite element modeling for buckling analysis of hybrid piezoelectric beam under electromechanical loads, Latin American Journal of Solids and Structures 11:770-789.

Rahman N., Alam M.N. (2015) Structural Control of Piezoelectric Laminated Beams under Thermal Load, Journal of Thermal Stresses 38:69–95.

Saravanos D.A., Heyliger P.R. (1995) Coupled layerwise analysis of composite beams with embedded piezoelectric sensors and actuators, Journal of Intelligent Material Systems and Structures 6:350-363.

Saravanos D.A., Heyliger P.R. (1999) Mechanics and computational models for laminated piezoelectric beams, plates and shells, ASME, Applied Mechanics Review 52:305 –320.

Sayyad A.S., Ghugal Y.M. and Shinde P.N. (2015a) Stress analysis of laminated composite and soft core sandwich beams using a simple higher order shear deformation theory, Journal of the Serbian Society for Computational Mechanics 9: 15-35.

Sayyad A.S., Ghugal Y.M., Naik N.S. (2015b) Bending analysis of laminated composite and sandwich beams according to refined trigonometric beam theory, Curved and Layer. Struct. 2:279–289.

Sunar M., Rao SS. (1999) Recent advances in sensing and control of flexible structures via piezoelectric materials technology, ASME, Applied Mechanics Review 52:1–16.

Tang Y.Y., Noor A.K., Xu K. (1996) Assessment of computational models for thermoelectroelastic multilayered plates. Computers and Structures 61:915 –933.

Yang J.S. (1999) Equations for thick elastic plates with partially electroded piezoelectric actuators and higher order electric fields, Smart Materials and Structures 8, 83–91.